UCRL-18545
cy. 2

University of California

Ernest O. Lawrence Radiation Laboratory

BUBBLE DENSITY MEASUREMENTS WITH HAZE

Giovanni Borreani, Dennis Hall, Loren Shalz, Phillip Hanson

October 28, 1968

DISCLAIMER

For International Conference on Advanced Data Processing for Bubble and Spark Chambers, Argonne, Illinois, Oct. 28-30, 1968

UCRL-18545
Preprint

UNIVERSITY OF CALIFORNIA

Lawrence Radiation Laboratory
Berkeley, California

AEC Contract No. W-7405-eng-48

BUBBLE DENSITY MEASUREMENTS WITH HAZE

Giovanni Borreani, Dennis Hall, Loren Shalz, Phillip Hanson

October 28, 1968

BUBBLE DENSITY MEASUREMENTS WITH HAZE

Giovanni Borreani*, Dennis Hall, Loren Shalz, Phillip Hanson

Iawrence Radiation Laboratory
University of California
Berkeley, California

28 October 1968

The following paper is the result of a collaborative effort between the Data Handling Group, headed by Howard White, and the Powell-Birge Physics Group, at UCLRL, Berkeley[1]. The development of the method was done by Howard White and Dennis Hall. The application of the method and the interpretation of the results was done by Giovanni Borreani. The programming was done by Loren Shalz and Phillip Hanson.

PURPOSE

The purpose of bubble density measurements in HAZE is to resolve the mass identification of events which are kinematically ambiguous, and to establish the correct mass of the charged particles in events for which two or more neutral particles are produced.

DATA

The HAZE program produces the following information for each track in each view measured.

T: The total number of times the track was traversed by the spot.

H: The total number of times the spot was sufficiently obscured to produce a digitizing. This number is usually referred to as the number of hits.

Mode: The mode of measurement. In the "normal" mode of measurement, the motion of the spot is perpendicular to the beam direction. In the "orthogonal" mode, the spot moves parallel to the beam direction. Although tracks may be measured in both modes, ionization information is only collected from the segment with the greater length in the direction of stage motion.

* On leave of absence from the Instituto di Fisca Nucleare - Seg. Li Torino, Italy.

In addition, the FOG program provides the following auxiliary information:

FMF: Film factor i.e., the tilt of the track with respect to the scan direction.

SPF: Space factor i.e., the tilt of the track in space with respect to the film plane.

$\bar{X},\bar{Y},\bar{Z}$: The space coordinates of the midpoint of the track.

FMF and SPF are defined as follows (See Figure 1):

Let

ΔX = the component of track length on film in the direction of stage motion.

L_{film} = the arc length of the track on the film.

L_{space} = the arc length of the track in space.

Then

$$FMF = \frac{\Delta X}{L_{film}} \quad \text{and} \quad SPF = \frac{L_{film}}{L_{space}}$$

BASIC METHOD

Following Strand[2] and others, we assume Poisson statistics. Therefore, The probability that digitizing does not occur on a single sweep is given by:

$P(\text{no hit}) = \exp\left[-k_F a\right]$, where

k_F = bubble density along the direction of stage motion, and

a = FSD spot size.

In hydrogen, the bubble density is known to vary with the particle velocity β as(3).

$$k = \frac{k_o}{\beta^2}, \text{ where}$$

k_o = the bubble density of a relativistic track.

We assume that the bubble density k in space is related to the bubble density k_F along the scan direction by:

$$k_F = \frac{k}{FMF \cdot SPF}$$

Thus we have

$$P(\text{hit}) \equiv HC = 1-\exp\left[\frac{-k_o a}{\beta^2 \cdot FMF \cdot SPF}\right]$$

Letting $c = k_o a$ we have

$$HC = 1-\exp\left[-\frac{c}{\beta^2 \cdot FMF \cdot SPF}\right]$$

The constraint c must be determined experimentally for each mode of measurement. An observed difference of about 30% is attributable to a difference in spot size between the two modes.

CALIBRATION

Determination of c is accomplished by requiring HC = H/T for particles of known velocity. For the normal mode of measurement, beam tracks were used. For the orthogonal mode a sample of kinematically unambiguous 4c events was used.

Having determined c for the two modes one may use H/T to predict the relative ionization. Figure 2 shows the relationship between the momentum and the relative ionization predicted by H/T. A sample of kinematically unambiguous 4c events was used. The two bands represent the pi and proton tracks.

Fitting these points to $1/\beta^x$ gives a value of x between 1.4 and 1.8 at 95% confidence limits. The explanation for this is not understood at this time although it is most probably due to some peculiarity in the chamber illumination system. In any case, the selection efficiency is not affected.

EXTENSION OF THE METHOD

It was seen that the above model was insufficient to describe the relationship between bubble density in space and H/T. In order to study this relationship further, the following quantities were developed:

$$HM_{IJ} = \frac{H_{IJ}}{T_{IJ}}$$

where I denotes the track and J denotes the view.

$$R_{IJ} = \frac{HM_{IJ}}{HC_{IJ}}$$

From a sample of tracks unambiguously defined by a 4c kinematical fit, scatter plots were made of R_{IJ} against all parameters which might affect the relationship. The parameters which were found to be significant were $\bar{X}$, $\bar{Y}$, $\bar{Z}$, and FMF. Figures 3, 4, 5, and 6 show the nature of these effects. The effects varied significantly with the mode of measurement and the view.

Improvements to HC_{IJ} are developed as follows:

For each mode and view find A_{IJ}, B_{IJ} such that

$$R_{IJ} = \frac{HM_{IJ}}{HC_{IJ}} \simeq A_{IJ} + B_{IJ}\cdot\bar{X} \equiv P_{IJ}(\bar{X})$$

This was done by hand fitting a line to the points in Figure 3.

The first improvement to HC_{IJ} is then given by:

$$HC^1_{IJ} = HC_{IJ}\cdot P_{IJ}(\bar{X})$$

Three more improvement cycles were performed as follows:

$$R^1_{IJ} = \frac{HM_{IJ}}{HC^1_{IJ}} \simeq C_{IJ} + D_{IJ}\cdot\bar{Y} + E_{IJ}\cdot(\bar{Y})^2 + F_{IJ}\cdot(\bar{Y})^3 \equiv Q_{IJ}(\bar{Y})$$

$$HC^2_{IJ} = HC^1_{IJ}\cdot Q_{IJ}(\bar{Y})$$

$$R^2_{IJ} = \frac{HM_{IJ}}{HC^2_{IJ}} \simeq G_{IJ} + H_{IJ}\cdot\bar{Z} + I_{IJ}\cdot(\bar{Z})^2 \equiv S_{IJ}(\bar{Z})$$

$$HC^3_{IJ} = HC^2_{IJ}\cdot S_{IJ}(\bar{Z})$$

$$R^3_{IJ} = \frac{HM_{IJ}}{HC^3_{IJ}} \simeq J_{IJ} + K_{IJ}\cdot FMF \equiv T_{IJ}(FMF)$$

$$HC^4_{IJ} = HC^3_{IJ}\cdot T_{IJ}(FMF)$$

Thus the final estimate HC^4_{IJ} is given by

$$HC^4_{IJ} = HC_{IJ}\cdot P_{IJ}(\bar{X})\cdot Q_{IJ}(\bar{Y})\cdot S_{IJ}(\bar{Z})\cdot T_{IJ}(FMF)$$

Figure 7 shows the $\bar{Z}$ dependence after all corrections have been made.

ERROR ON HM

The error on HM_{IJ} is given by:

$$\Delta HM_{IJ} = \sqrt{\frac{HM_{IJ}(1-HM_{IJ})}{T} + C_2^2}$$

where $\frac{HM_{IJ}(1-HM_{IJ})}{T}$ is the statistical error, and C_2 is an emperical constant determined from the dispersion of HM on heavily ionizing tracks. The expression for ΔHM_{IJ} is under study at this time. A possible improvement would be to use

$$\Delta HM_{IJ} = \sqrt{\frac{HC^4_{IJ}(1-HC^4_{IJ})}{T} + C_2^2}$$

IONIZATION χ^2

In addition to the above corrections, it was found that variations in chamber operating conditions produced an overall shift in the relationship between HC_{IJ} and HM_{IJ}. Figure 8 shows the variation of HM_{IJ}(for 1.6 GeV/c beam tracks) with time (roll number).

For this reason, a normalization factor $\bar{k}$ was introduced for each event. It was assumed that within a frame HM_{IJ} would vary with HC^4_{IJ} as:

$$HM_{IJ} = \bar{k}\ (HC^4_{IJ} - 1) + 1$$

which corresponds to a straight line through the point $HM_{IJ} = 1$, $HC^4_{IJ} = 1$.

We define the normalized deviation $G_{IJ}(\bar{k})$ by

$$G_{IJ}(\bar{k}) = \frac{\bar{k}(HC^4_{IJ}-1) + 1 - HM_{IJ}}{\Delta HM_{IJ}}$$

The normalization factor $\bar{k}$ is then determined for each event by minimizing $\Sigma_{IJ}\ G_{IJ}(\bar{k})^2$ excluding beam tracks for which $(HM_{IJ}-HC^4_{IJ})/\Delta HM_{IJ} > 3.0$. The purpose for excluding these tracks is to remove the contamination of superimposed beam tracks which will show artificially high values of HM_{IJ}.

Once the normalization factor has been determined for the event, the ionization χ^2 is developed. For each track, a "best" view is selected:

1) For beam tracks, the view with the largest value of T.

2) For non-beam tracks, the view with the largest value of FMF·SPF i.e., the view which is best "seen" by the FSD.

The ionization χ^2 is then taken as

$\chi^2_{ION} = \sum_I G^2_{IJ*}$, where J* is the "best" view.

Figure 9 shows the distribution of χ^2_{ION} for unambiguously identified 4c π^+ 4 prongs at 1.6 GeV/c. Figure 10 shows the distribution of χ^2_{ION} for unambiguously identified 4c π^+ 4 prongs at 3.5 GeV/c.

The methods used for the two experiments were somewhat different. At the time of the 3.5 GeV/c experiment, ionization information was only available from one view, picked on the basis of having the largest value of T. The ionization χ^2 was defined to be $\chi^2_{ION}/5$. The loss of information from the other two views was detrimental to both the chi-square distribution and the selection efficiency.

METHOD OF SELECTION

For those events which are kinematically ambiguous, the ionization χ^2 of the competing hypotheses are tested. For the 1.6 GeV/c experiment if χ^2_{ION} is less than 15.0 for one hypothesis and greater than 15.0 for all other competing hypotheses, a selection is made. Otherwise, the event remains ambiguous. For the 3.5 GeV/c experiment the cutoff is 7.0.

RESULTS

Figure 11 shows the relationship between the momentum of the pion and the proton for those events which have a 4c kinematical ambiguity. Clearly the kinematically ambiguous events have two positive tracks at the same momentum. The sample is from the 1.6 GeV/c π^+ exposure.

Figure 12 shows the relationship between the pion momentum and the proton momentum for those events in which a selection is made on the basis of ionization χ^2. Selections are made over the full range of momenta which corresponds to a selection in relative ionization of 1.92 from 1.02. Figure 13 shows the relationship between the ionization χ^2 of the two competing 4c hypotheses for the 1.6 GeV/c π^+ exposure. The clustering at points along

the two axes gives an indication of the selection efficiency.

Figure 14, 15 and 16 are the corresponding plots for the 3.5 GeV/c π^+ exposure. Selections are made up to 1.90 GeV/c which corresponds to a selection in relative ionization of 1.24 from 1.00.

Table 1 shows the selection efficiency for the 3.5 GeV/c π^+ exposure where only one view was available. Table 2 shows the selection efficiency for the 1.6 GeV/c π^+ exposure where all three views were available.

ACKNOWLEDGEMENTS

We are grateful to Donna Chrisler for her energetic help with the programming.

REFERENCES

(1) For an earlier work on this subject see G. Borreani - D. Hall, Calibration of FSD Ionization Measurements in Hydrogen 11/28/67. PB Memo - 119.

(2) A detailed discussion of this method can be seen in: R. C. Strand, Bubble Density Measurements with the Hough-Powell Digitizer. BNL Bubble Chamber Report G-34, January 1963.

(3) See for example C. Peyrou, International Conference on Instrumentation for High Energy Physics, Berkeley, Calif. Sept. 1960 - or B. Sechi-Zorn and G. T. Zorn, Suppl. Nuovo Cim 26, 197, 1962.

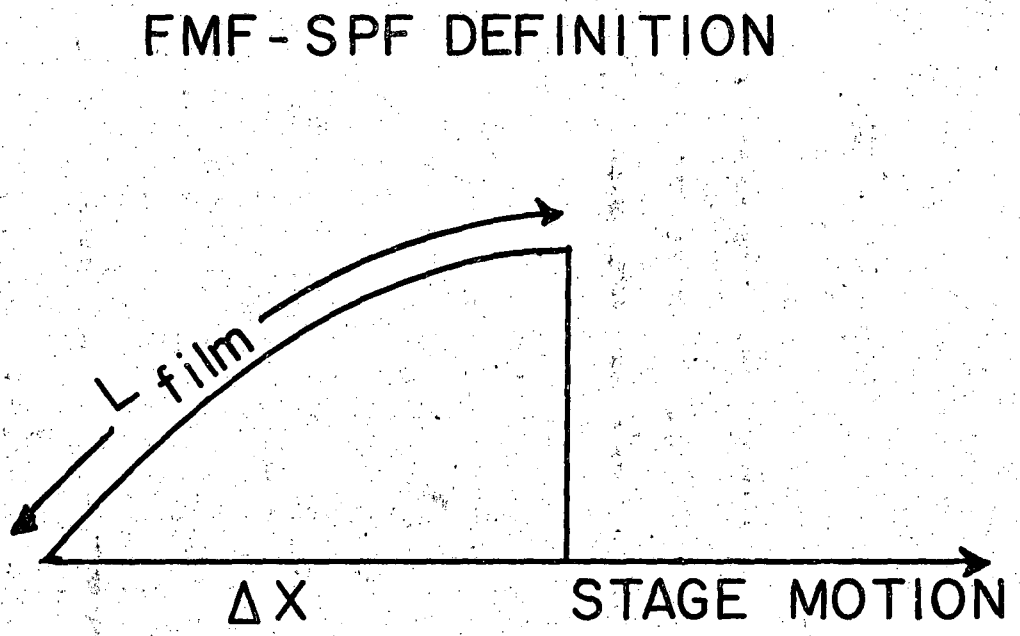

Fig. 1. XBL 6810-6021

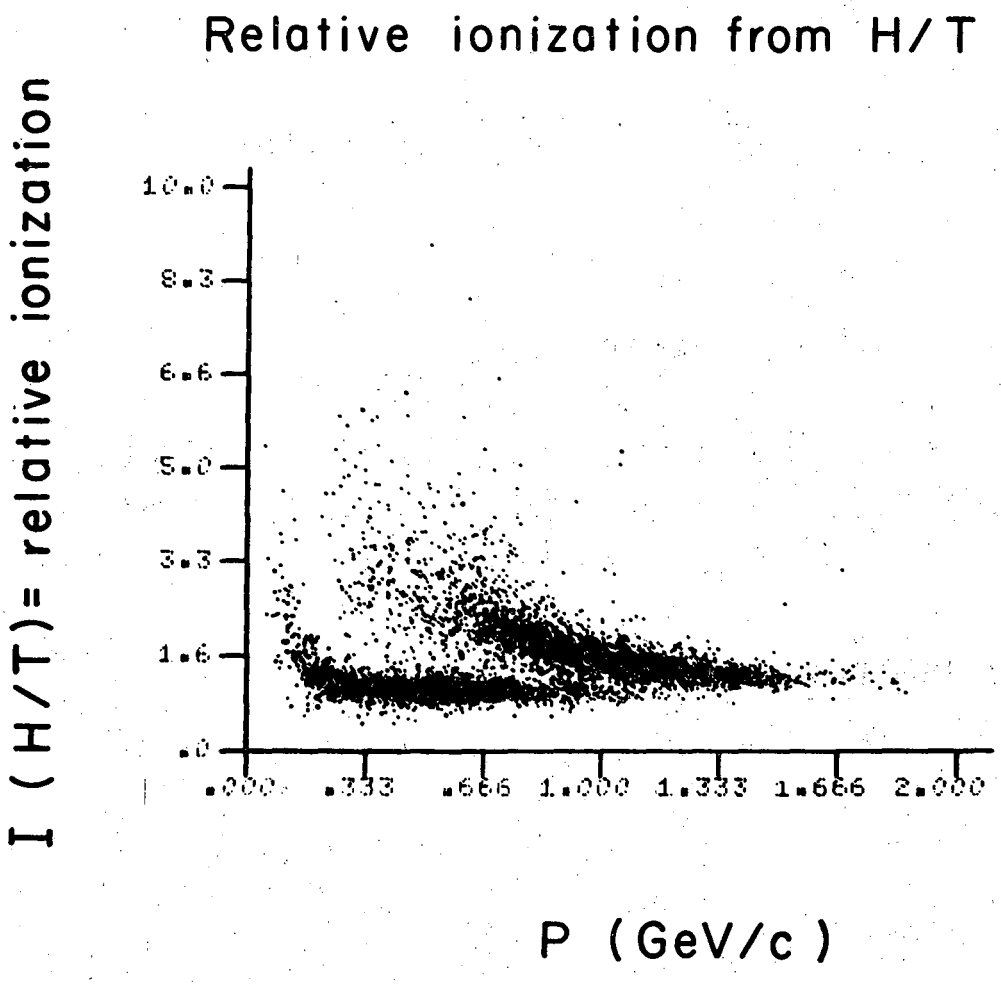

2135 tracks, normal mode, view 1; kinematically unambiguous 4C events at 1.6 GeV/c.

Fig. 2. XBL6810-6925

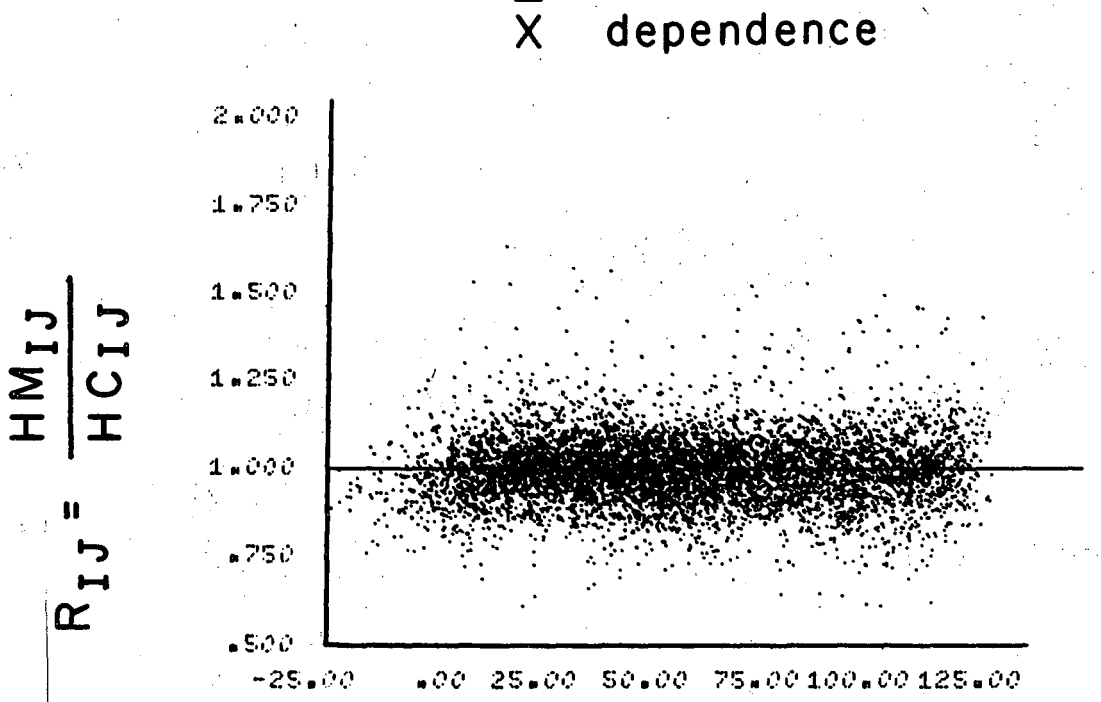

5884 tracks, normal mode, view 1; kinematically unambiguous 4C events at 1.6 GeV/c.

Fig. 3. XBL6810-6926

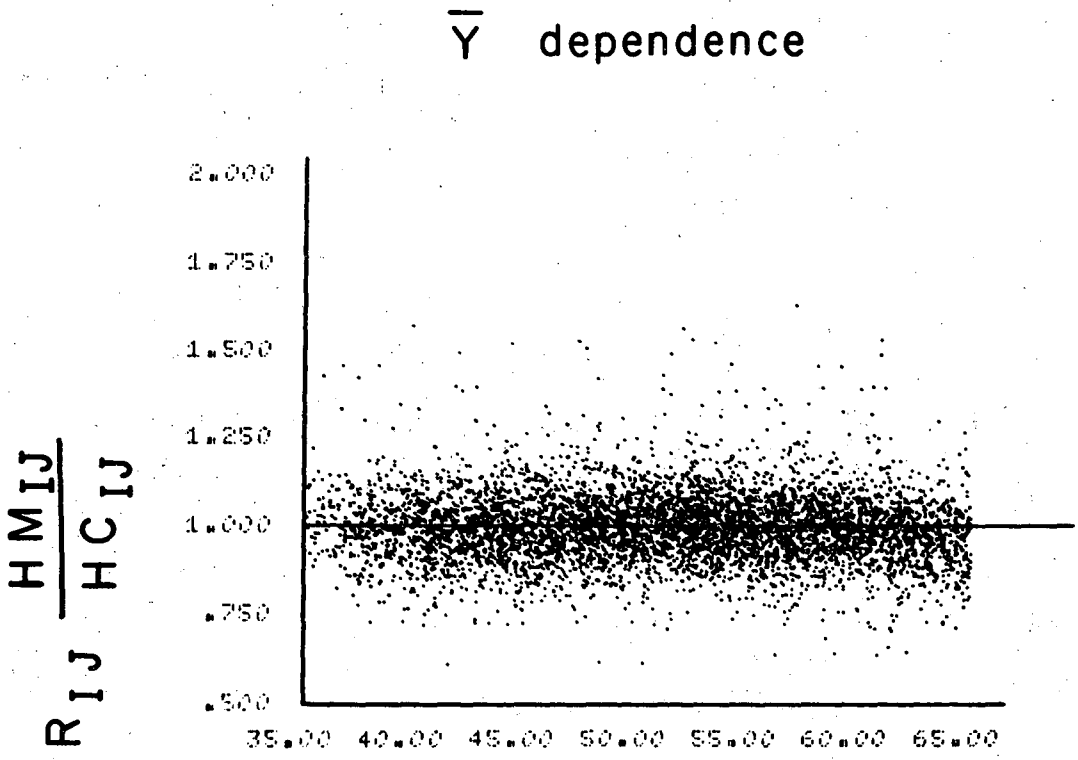

Fig. 4. XBL6810-6927

$\bar{Z}$ dependence

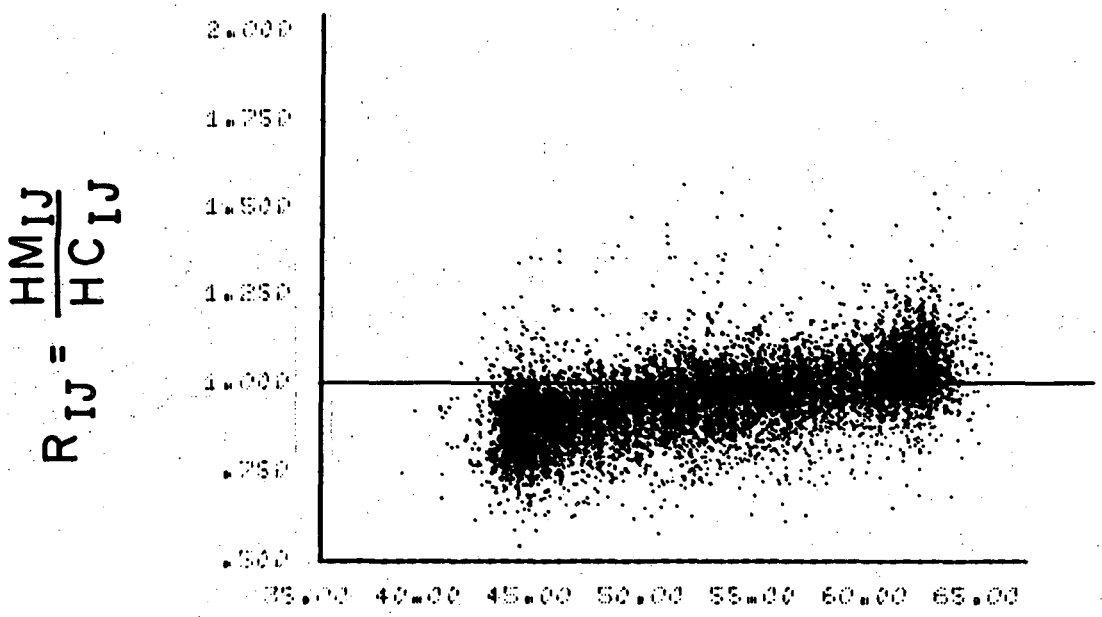

$\bar{Z}$ (cm space)

8673 tracks, normal mode, view 1; kinematically unambiguous 4C events at 1.6 GeV/c.

Fig. 5. XBL6810-6928

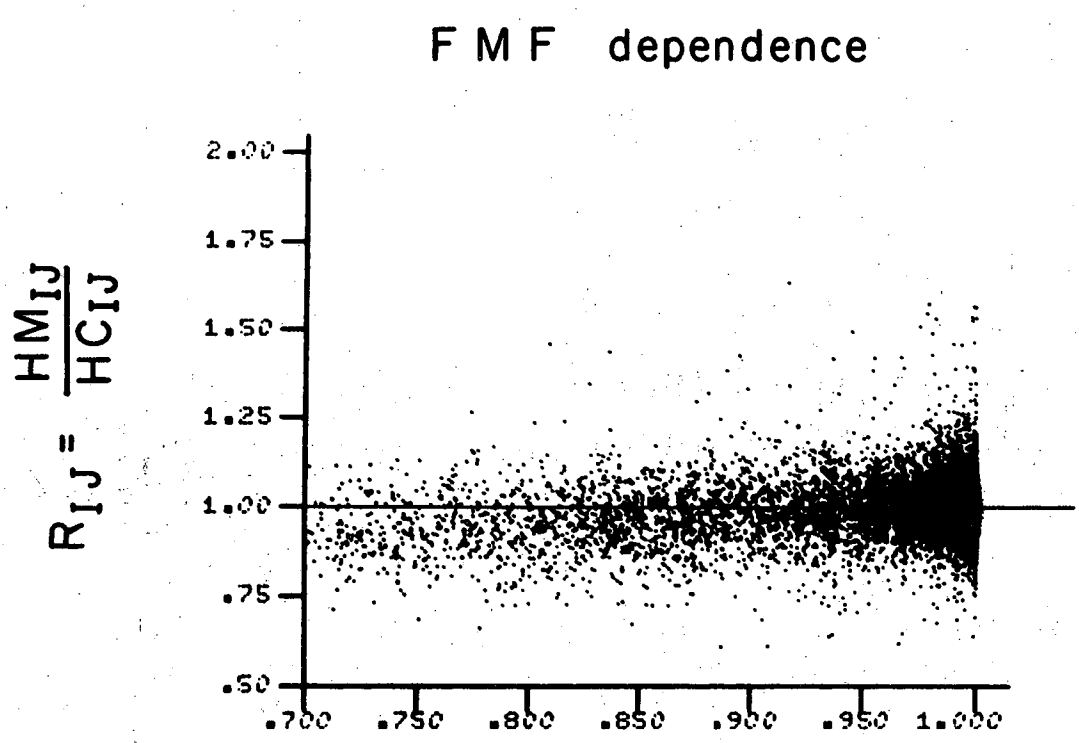

Fig. 6. XBL6810-6929

$\bar{Z}$ dependence after corrections

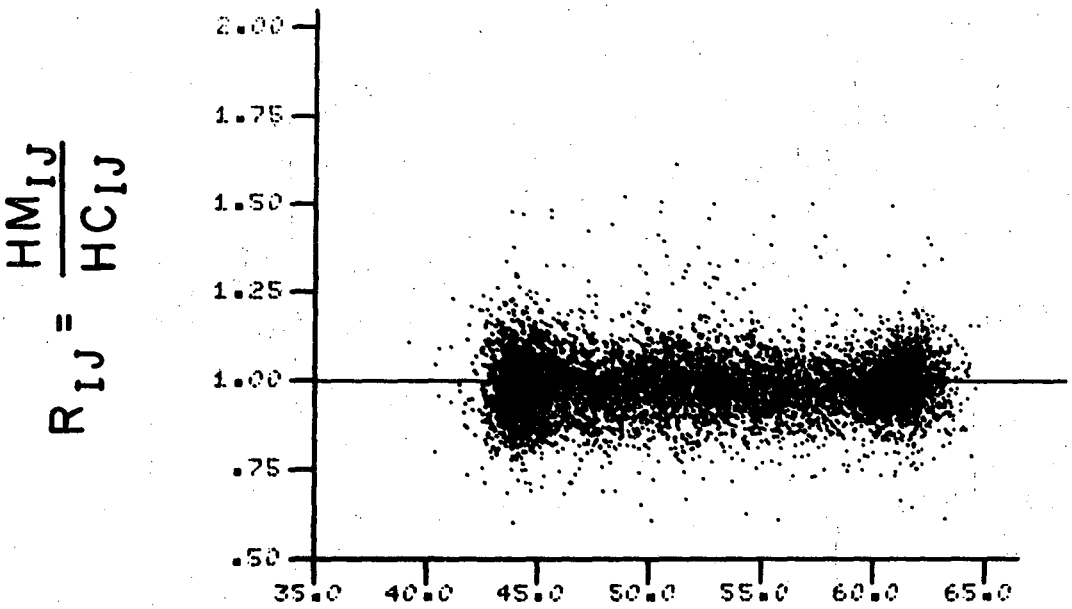

5474 tracks, normal mode, view 1; kinematically unambiguous 4C events at 1.6 GeV/c.

Fig. 7. XBL6810-6930

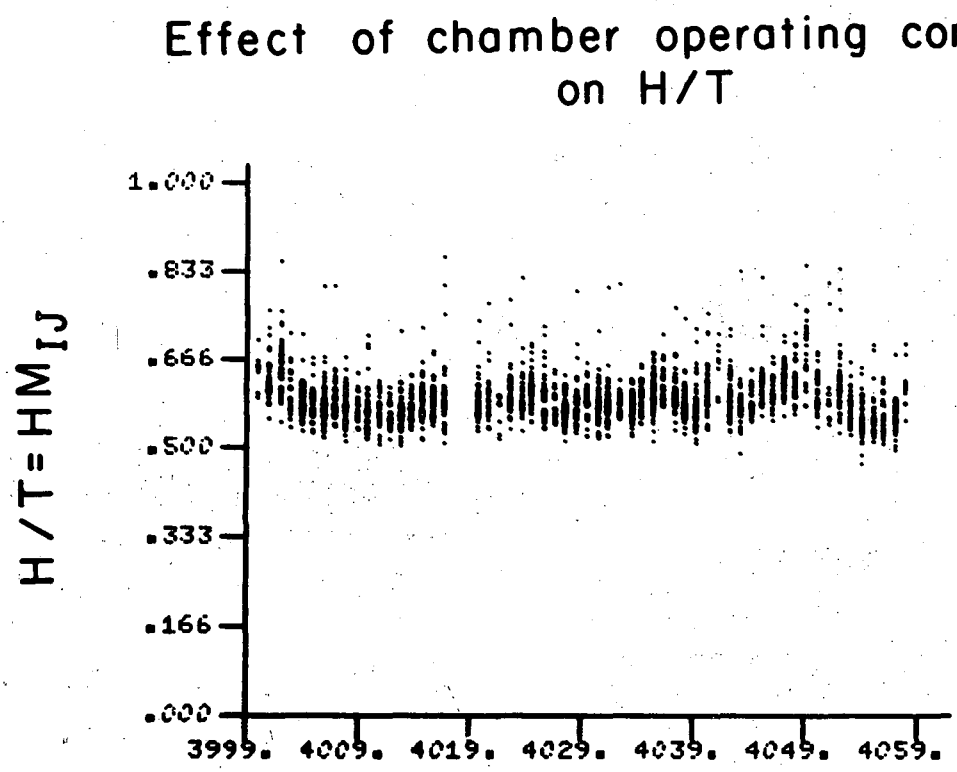

Fig. 8. XBL6810-6931

Distribution of χ^2_{ion} at 1.6 GeV/c

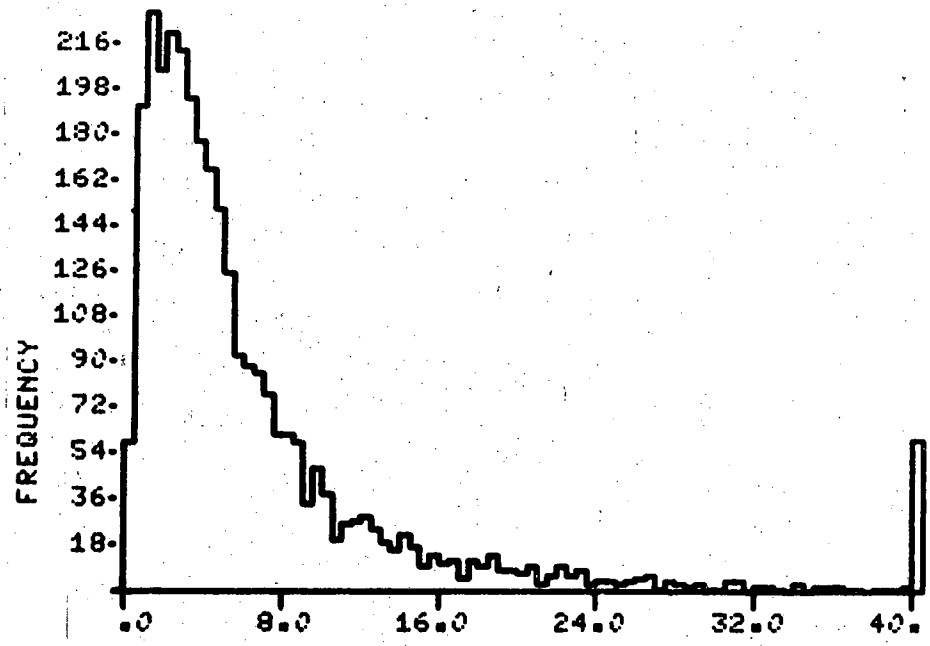

$$\chi^2_{ion} = \sum_I G^2_{IJ}*$$

3055 kinematically unambiguous 4C events.
Ionization measurements – 3 views.

Fig. 9. XBL 6810-6932

Distribution of χ^2_{ion} at 3.5 GeV/c

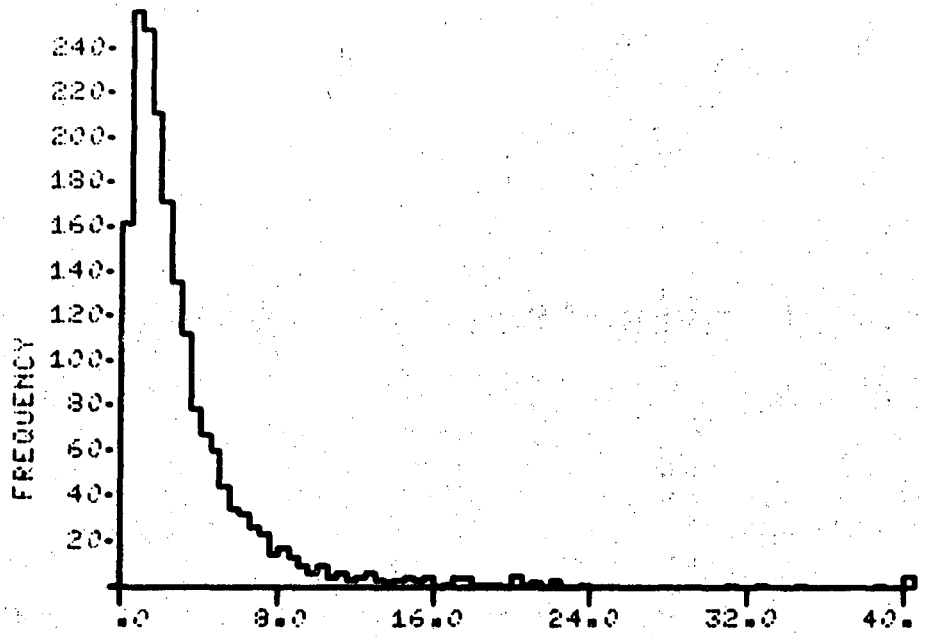

$$\chi^2_{ion} = \sum_I G^2_{IJ*}/5$$

1801 kinematically unambiguous 4C events.
Ionization measurements – 1 view only.

Fig. 10. XBL6810-6933

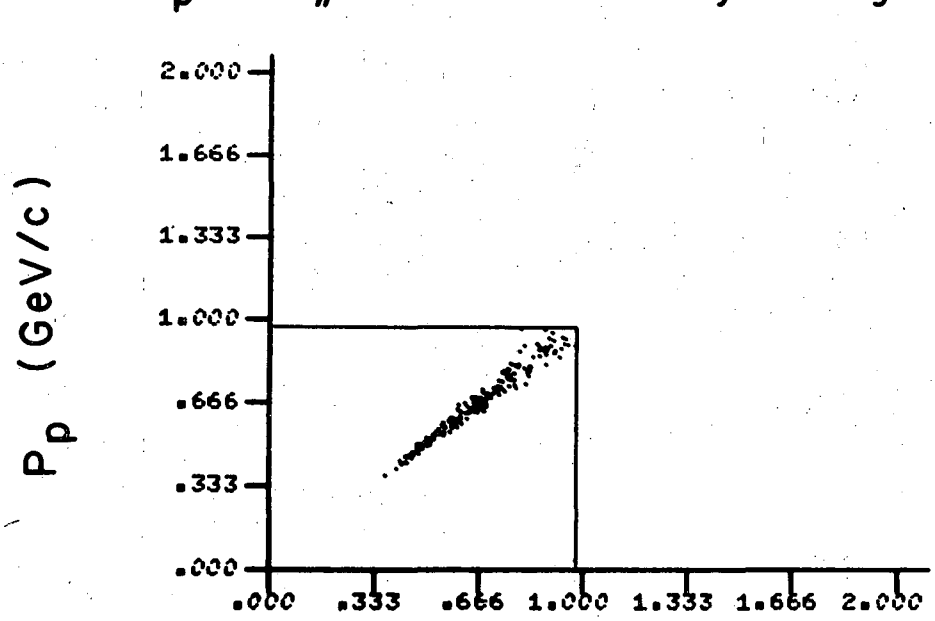

Fig. 11. XBL6810-6934

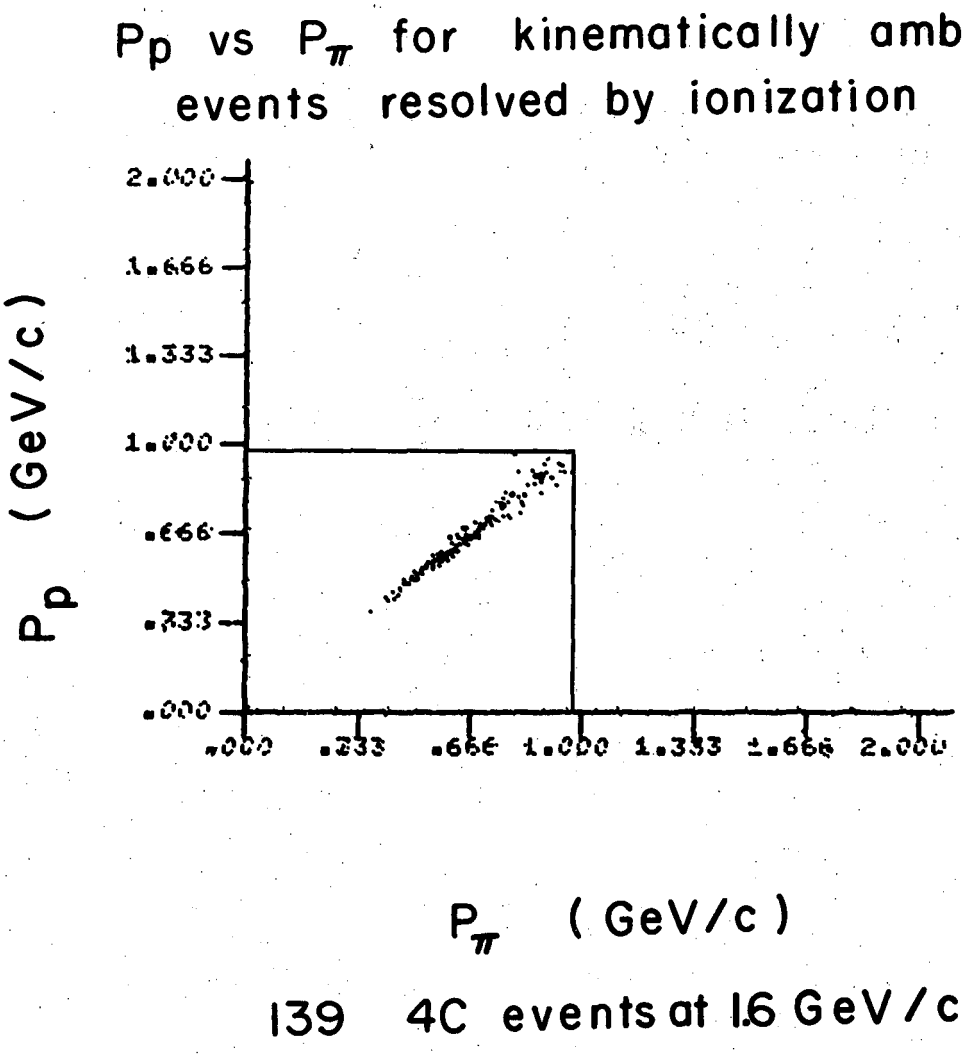

Fig. 12. XBL6810-6936

Efficiency of selection by χ^2_{ion} between competing 4C hypotheses

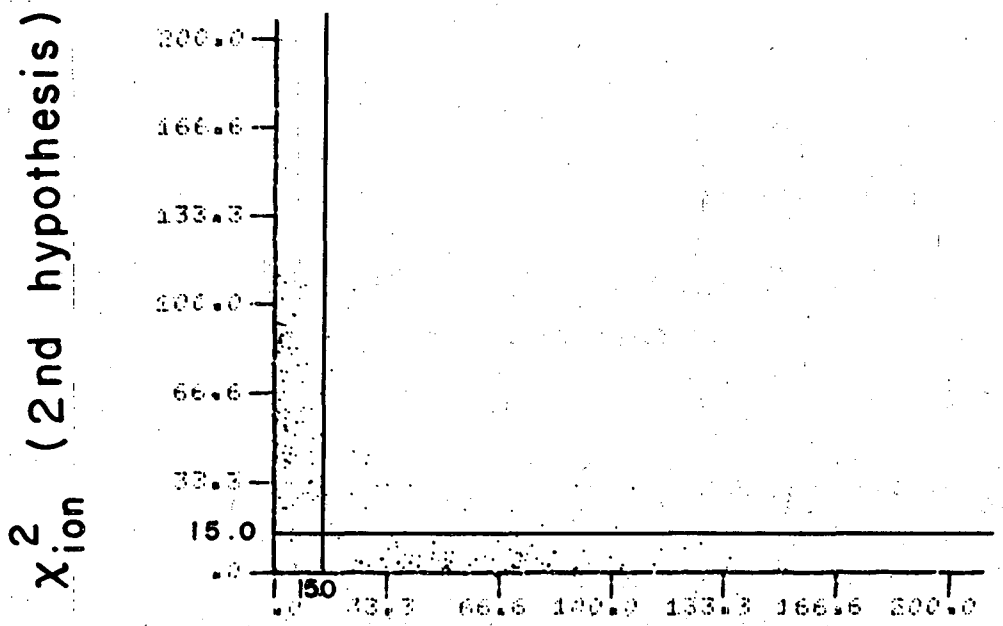

197 kinematically ambiguous events at 1.6 GeV/c
Ionization measurements – 3 views.

Fig. 13. XBL6810-6937

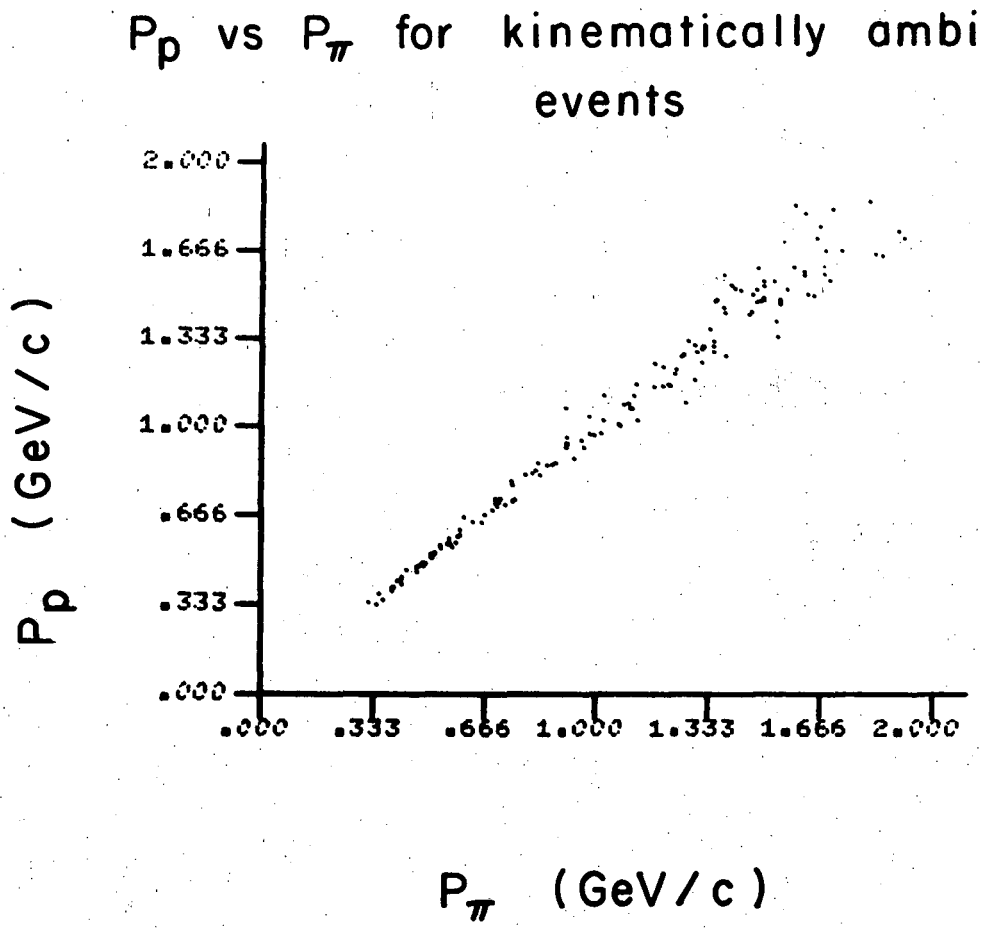

Fig. 14. XBL6810-6939

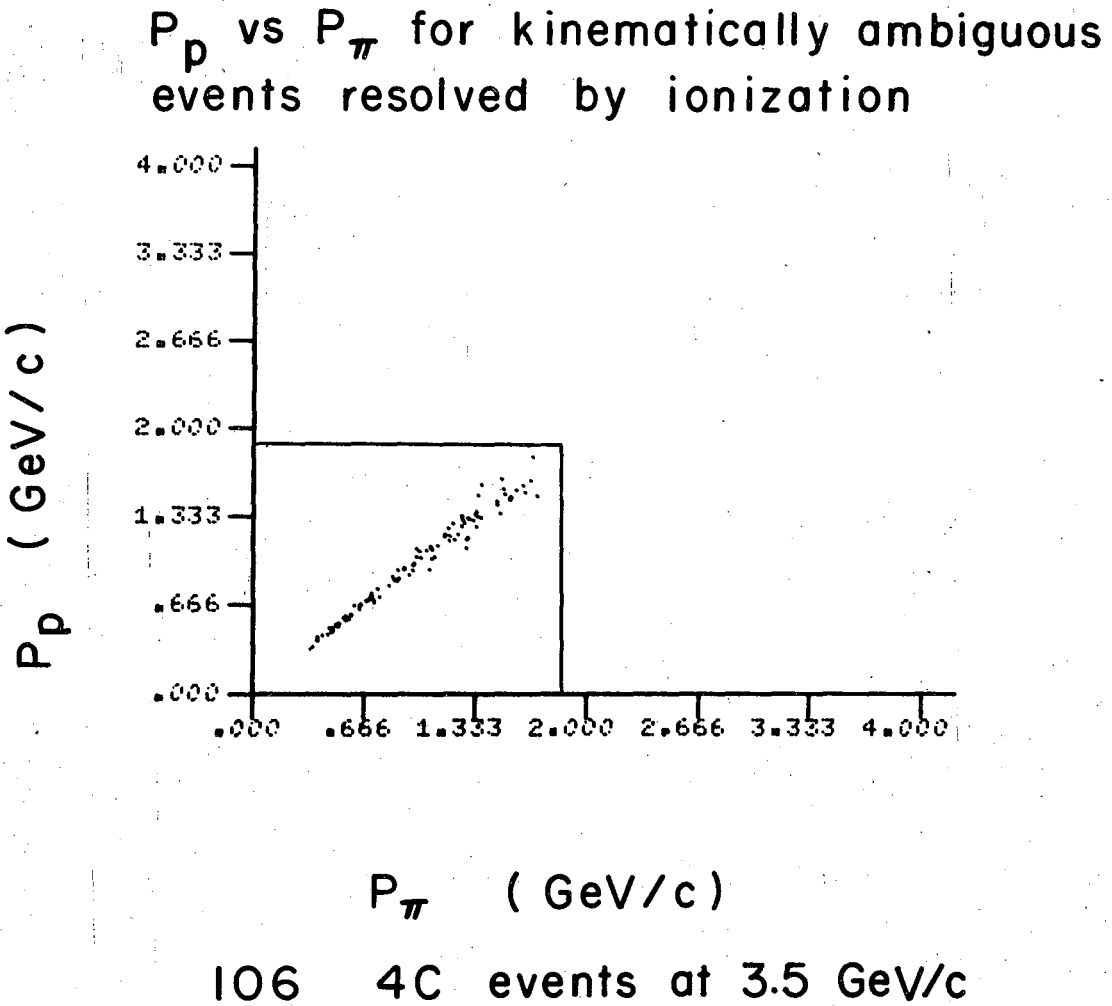

Fig. 15. XBL6810-6940

Efficiency of selection by χ^2_{ion} between competing 4C hypotheses

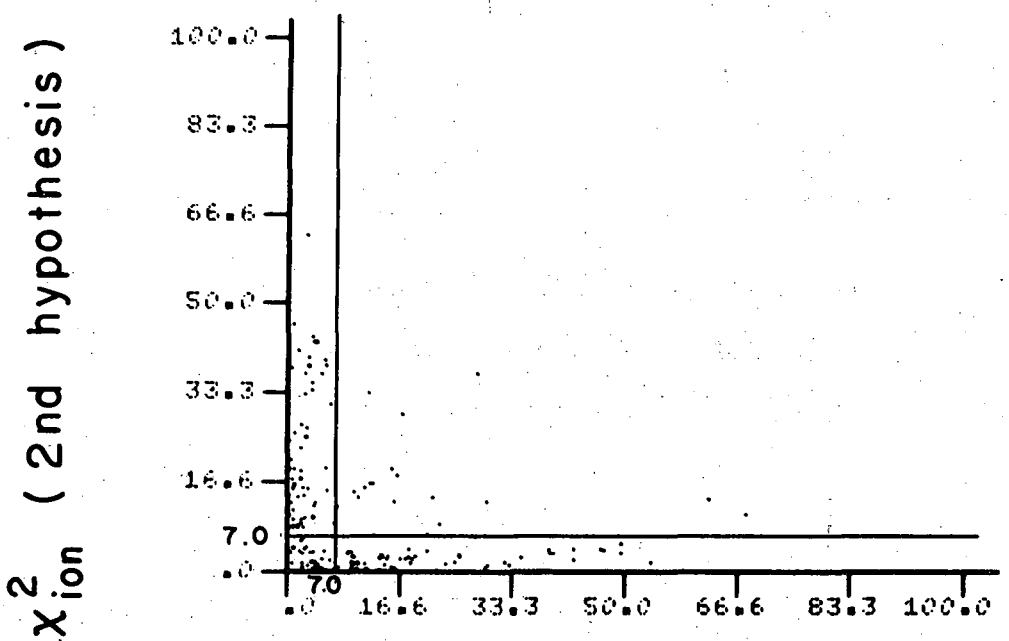

165 kinematically ambiguous 4C events at 3.5 GeV/c
Ionization measurements – 1 view only

Fig. 16. XBL6810-6941

Table 2. Resolution efficiency of kinematically ambiguous events by ionization measurement; 1.6 GeV/c, π^+ exposure, 72" HBC.

4548 events
3900 kinematically unique
648 kinematically ambiguous

Category	Number of events		Resolution efficiency (%)
	Kinematically ambiguous	Resolved by ionization	
4C–4C (no 1C)	173	154	89
4C–1C	254	210 as 4C 0 as 1C	83
1C–1C (no 4C)	221	172	78
Total	648	536	83

Ionization measurements from all three views.